High Dynamic Range Imaging: Spatially Varying Pixel Exposures*

Shree K. Nayar
Department of Computer Science
Columbia University, New York, U.S.A.
nayar@cs.columbia.edu

Tomoo Mitsunaga
Media Processing Laboratories
Sony Corporation, Tokyo, Japan
mitsunag@av.crl.sony.co.jp

Abstract

While real scenes produce a wide range of brightness variations, vision systems use low dynamic range image detectors that typically provide 8 bits of brightness data at each pixel. The resulting low quality images greatly limit what vision can accomplish today. This paper proposes a very simple method for significantly enhancing the dynamic range of virtually any imaging system. The basic principle is to simultaneously sample the spatial and exposure dimensions of image irradiance. One of several ways to achieve this is by placing an optical mask adjacent to a conventional image detector array. The mask has a pattern with spatially varying transmittance, thereby giving adjacent pixels on the detector different exposures to the scene. The captured image is mapped to a high dynamic range image using an efficient image reconstruction algorithm. The end result is an imaging system that can measure a very wide range of scene radiances and produce a substantially larger number of brightness levels, with a slight reduction in spatial resolution. We conclude with several examples of high dynamic range images computed using spatially varying pixel exposures.

1 High Dynamic Range Imaging

Any real-world scene has a significant amount of brightness variation within it. The human eye has a remarkable dynamic range that enables it to detect subtle contrast variations and interpret scenes under a large variety of illumination conditions [Blackwell, 1946]. In contrast, a typical video camera, or a digital still camera, provides only about 8 bits (256 levels) of brightness information at each pixel. As a result, virtually any image captured by a conventional imaging system ends up being too dark in some areas and possibly saturated in others. In computational vision, it is such low quality images that we are left with the task of interpreting. Clearly, the low dynamic range of existing image detectors poses a severe limitation on what computational vision can accomplish. This paper presents a very simple modification that can be made to any conventional imaging system to dramatically increases its dynamic range. The availability of extra bits of data at each image pixel is expected to enhance the robustness of vision algorithms.

*This work was supported in part by an ONR/DARPA MURI grant under ONR contract No. N00014-97-1-0553 and in part by a David and Lucile Packard Fellowship. Tomoo Mitsunaga is supported by the Sony Corporation.

2 Existing Approaches

First, we begin with a brief summary of existing techniques for capturing a high dynamic range image with a low dynamic range image detector.

2.1 Sequential Exposure Change

The most obvious approach is to sequentially capture multiple images of the same scene using different exposures. The exposure for each image is controlled by either varying the F-number of the imaging optics or the exposure time of the image detector. Clearly, a high exposure image will be saturated in the bright scene areas but capture the dark regions well. In contrast, a low exposure image will have less saturation in bright regions but end up being too dark and noisy in the dark areas. The complementary nature of these images allows one to combine them into a single high dynamic range image. Such an approach has been employed in [Azuma and Morimura, 1996], [Saito, 1995], [Konishi *et al.*, 1995], [Morimura, 1993], [Ikeda, 1998], [Takahashi *et al.*, 1997], [Burt and Kolczynski, 1993], [Madden, 1993] [Tsai, 1994]. In [Mann and Picard, 1995], [Debevec and Malik, 1997] and [Mitsunaga and Nayar, 1999] this approach has been taken one step further by using the acquired images to compute the radiometric response function of the imaging system.

The above methods are of course suited only to static scenes; the imaging system, the scene objects and their radiances must remain constant during the sequential capture of images under different exposures.

2.2 Multiple Image Detectors

The stationary scene restriction faced by sequential capture is remedied by using multiple imaging systems. This approach has been taken by several investigators [Doi *et al.*, 1986], [Saito, 1995], [Saito, 1996], [Kimura, 1998], [Ikeda, 1998]. Beam splitters are used to generate multiple copies of the optical image of the scene. Each copy is detected by an image detector whose exposure is preset by using an optical attenuator or by changing the exposure time of the detector. This approach has the advantage of producing high dynamic range images in real time. Hence, the scene objects and the imaging system are free to move during the capture process. The disadvantage of course is that this approach is expensive as it requires multiple image detectors, precision optics for the alignment of all the acquired images and additional hardware for the capture and processing of multiple images.

2.3 Multiple Sensor Elements Within a Pixel

A rather novel approach to high dynamic range imaging uses a different CCD design. In this approach, each detector cell includes two sensing elements (potential wells) of different sizes (and hence sensitivities). When the detector is exposed to the scene, two measurements are made within each cell and they are combined on-chip before the image is read out. Such an approach has been proposed by [Street, 1998], [Handy, 1986], [Wen, 1989], [Hamazaki, 1996], [Murakoshi, 1994] and [Konishi *et al.*, 1995]. However, this technique is expensive as it requires a sophisticated detector to be fabricated. In addition, spatial resolution is reduced by a factor of two since the two potential wells take up the same space as two pixels in a conventional image detector. Further, the technique is forced to use a simple combining technique for the outputs of the two wells as it is done on-chip.

2.4 Adaptive Pixel Exposure

A different approach to high dynamic range imaging has been proposed in [Brajovic and Kanade, 1996]. Here, a novel solid state image sensor is developed where each pixel on the device includes a computational element that measures the time it takes to attain full potential well capacity. Since the full-well capacity is the same for all pixels, the time to achieve it is proportional to image irradiance. The recorded time values are read out and converted to a high dynamic range image. This approach is attractive, but faces the challenge of scaling to high resolution while keeping fabrication costs under control. In addition, since exposure times can be large in dark scene regions, the method is expected to be more susceptible to motion blur. This work is in progress and an initial version of the device with 32x32 cells has been implemented.

3 Spatially Varying Pixel Exposures

In this paper, we introduce the notion of spatially varying pixel sensitivities for high dynamic range imaging. Consider the array of pixels shown in Figure 1. The brightness level associated with each pixel represents its sensitivity, such that, the brighter pixels have greater exposure to image irradiance and the darker ones have lower exposure. In the example shown, four neighboring pixels have different exposures ($e_0 < e_1 < e_2 < e_3$) and this pattern is repeated over the detector array. We will refer to the captured image as a spatially varying exposure (SVE) image.

The key feature here is that we are simultaneously sampling the spatial dimensions as well as the exposure dimension of image irradiance. Note that when a pixel is saturated in the acquired image, it is likely to have a neighbor that is not, and when a pixel produces zero brightness, it is likely to have a neighbor that produces non-zero brightness. Our goal is to exploit this spatio-exposure sampling and compute a high dynamic range image of the scene.

It is worth noting that we are by no means restricted to the pattern shown in Figure 1. The number of discrete exposures can differ and the pattern does not have to be periodic. There may be instances where a random exposure pattern may be useful. The pattern can be implemented in many ways. One approach is to place a mask with cells

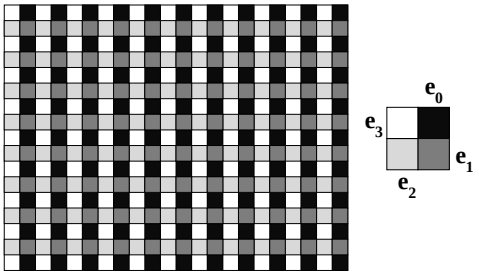

Figure 1: Pixel exposures (or sensitivities) can be spatially varied to simultaneously sample scene radiance along spatial as well as dynamic range dimensions. The captured image is used to compute a high dynamic range image of the scene.

of different optical transparencies adjacent to the detector array. This pattern can also be etched directly on the detector in the case of solid state devices such as CCDs. Alternatively, the sensitivity of the pixels can be preset by using different microlenses on the array, by using different integration times for different pixels, or by embedding different apertures for the potential wells of the pixels. All these implementations result in the same effect, namely, a detector array with spatially varying exposures.

In this paper, we will assume the use of an optical mask with a pattern of cells with different transparencies, as this approach results in a very simple modification to virtually any imaging system. Figure 2 shows several ways of incorporating an optical mask into an imaging systems. In Figure 2(a), the mask is placed adjacent to the detector plane. In cases where access to the detector plane is difficult, the mask may be placed outside the imaging lens. In this case, a primary lens is used to focus the scene onto the mask plane. The light rays that emerge from the mask are received by the imaging lens and focused onto the detector plane. A diffuser may be used to remove the directionality of rays arriving at the mask. Then the imaging lens is focused at the diffuser plane. Figure 2(c) shows how a mask can be easily incorporated into a photographic camera as well. In this case, the mask is fixed adjacent to the plane along which the film advances. Finally, the SVE idea is by no means restricted to visible light. In principle, the dynamic range of any electromagnetic radiation imager can be enhanced using this method.

4 Dynamic Range

Let us consider the case where scene radiance is smoothly varying such that adjacent pixels are subjected to roughly the same radiance. It is important to note that we are making this assumption only for the purpose of illustration and that the SVE method *does not* rely on such an assumption. Consider an SVE imaging system that uses a CCD image detector. The dynamic range of the CCD detector itself can be defined as the ratio of the maximum and the minimum electron charge measurable by the potential wells corresponding to the pixels [Theuwissen, 1995],[Healey and Kondepudy, 1994]. Dynamic range is often expressed as:

$$DR \;=\; 20 \log \frac{C_{full}}{N_r}\,, \qquad (1)$$

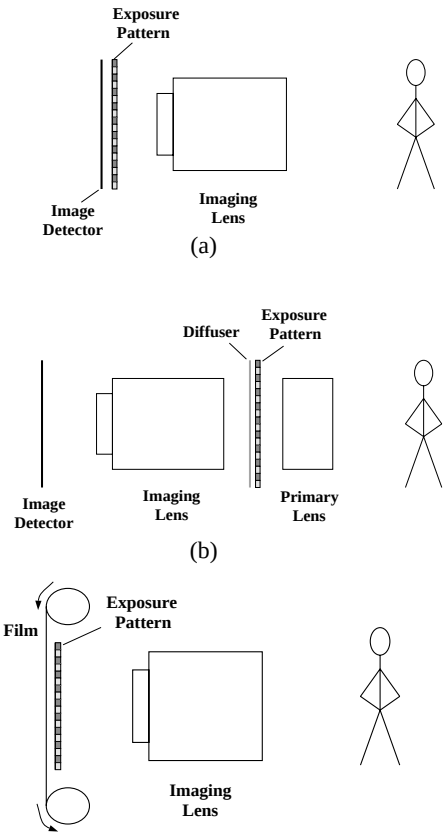

Figure 2: One way to achieve spatially varying pixel exposures is by using an optical mask with an array of cells with different transparencies. (a) Such a mask can be placed adjacent to the image detector array. (b) The mask can also be fixed at a distance from the detector by using a primary lens to focus scene rays onto the mask and an imaging lens to project radiance at the mask onto the detector plane. (c) For film cameras, the mask can be placed adjacent to the film area that is exposed to the scene.

where C_{full} represents the full-well capacity of the detector and N_r is rms of the read-noise of the CCD. The analog output of the camera is subsequently quantized via A/D conversion to obtain a digital image. The number of gray levels in the image and the gain of the A/D convertor are usually adjusted such that the maximum gray level I_{max} corresponds to the full-well capacity and the minimum level I_{min} corresponds to the minimum signal (read-noise) detectable by the CCD. The process of quantization itself introduces an additional noise, but we will ignore its contribution for simplicity. Then, the dynamic range of the digitized image can be written as:

$$DR = 20 \log \frac{I_{max}}{I_{min}} . \qquad (2)$$

Hence, the number of gray levels is often viewed as a measure of the dynamic range. The minimum gray level I_{min} is typically set to 1. Therefore, an 8-bit CCD detector results in a dynamic range of $20 \log 255 = 48.13$ decibels.

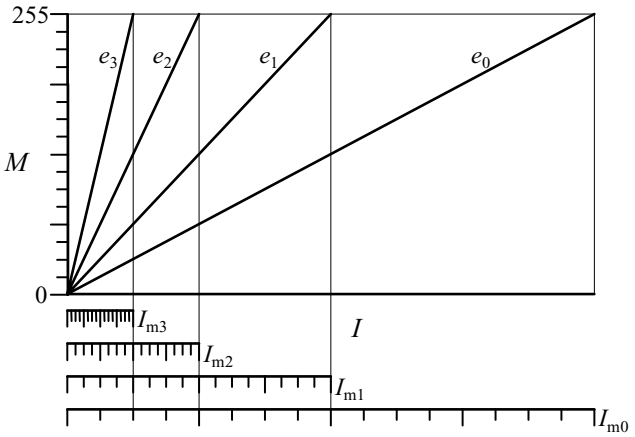

Figure 3: An imaging system with a spatially varying exposure pattern simultaneously measures local scene radiance I using different exposures. In the pattern shown in Figure 1, four exposures are used such that the maximum exposure e_3 measures low scene radiance with high fidelity, while the minimum exposure e_0 can measure very high radiance values without saturation. When information from the four exposures are used together, a non-linear quantization of scene radiance is obtained.

In the case of an SVE camera, the minimum gray level remains $I_{min} = 1$, but the maximum detectable gray level becomes $I_{max}\, e_{max}/e_{min}$ where e_{max} and e_{min} are the maximum and minimum exposures used in the exposure pattern. Hence, the dynamic range of an SVE camera is

$$DR_{sve} = 20 \log \frac{I_{max}}{I_{min}} \frac{e_{max}}{e_{min}} \qquad (3)$$

In Figure 1, we have four exposures. Let us assume these are $e_3 = 4e_2 = 16e_1 = 64e_0$. Then, the dynamic range is $20 \log (255 \times 64) = 84.25$ decibels, which is a dramatic increase with respect to a conventional imaging system.

5 Number of Gray Levels

As seen from Figure 3, each exposure is uniformly quantized but the set of four exposures together produce a non-uniform quantization of scene radiance. As noted by Madden [Madden, 1993], this non-uniformity can be advantageous as it represents a judicious allocation of resources (bits). Though the difference between quantization levels increases with scene radiance, the sensitivity to contrast remains more or less linear. This is because contrast is defined as brightness change normalized by brightness itself.

We now determine the total number of gray levels captured by an SVE imaging system. Let the total number of quantization levels produced at each pixel be q (256 for a 8-bit detector) and the number of different exposures in the pattern be K. Then, as seen from Figure 3, a total of $q\,K$ levels lie within the range of measurable radiance values. However, as seen from the figure, the output ranges of the different exposures overlap with each other and, for certain sets of exposures, the quantization levels for the

different exposures can exactly coincide in the overlap regions. Thus, one may consider only the quantization levels contributed by the highest exposure within any given overlap region. Then, the total number of unique quantization levels can be determined to be:

$$Q \;=\; q \;+\; \sum_{k=0}^{K-1} R\left((q-1) - (q-1)\frac{e_k}{e_{k-1}}\right), \quad (4)$$

where $R(x)$ rounds-off x to the closest integer. For an 8-bit detector with an SVE pattern with four exposures such that $e_k = 4e_{k-1}$, the total number of unique quantization levels is found to be $Q = 869$, which is a considerable improvement over $q = 256$ for just the image detector.

6 Spatial Resolution

In a conventional imaging system, the number of sensing elements (pixels) on the detector and the field of view that is projected by the imaging optics onto the detector determine the spatial resolution of the system. It is important to note that in a SVE imaging system the number of pixels remain the same and therefore there is no loss in resolution due to the sampling process. However, a reduction in resolution results from the fact that some of the pixels with high exposure are expected to be saturated and some of the ones with very low exposure are expected to produce low and noisy intensities. The goal here is to reconstruct a high dynamic range image despite the presence of these saturated and low intensity measurements. We will briefly describe two algorithms for this purpose.

6.1 Image Reconstruction by Aggregation

The simplest approach is to average the local brightness values produced by different exposures. At first glance, this might appear to be a crude approach to the problem. However, it has desirable dynamic range attributes and does not reduce resolution as much as one might expect.

Let us assume that the captured SVE image is $M(i,j)$ and the reconstructed high dynamic range image is $M_r(i,j)$. Consider the exposure pattern shown in Figure 1. The aggregation method simply convolves the captured image with a 2×2 box filter, which yields the average of the four brightness values it is applied to. This average value is assigned to center of the four pixels, thereby producing an image that is offset from the original image by half the distance between pixels, in each of the two dimensions.

Note that any 2×2 set of pixels in the SVE image will include pixels with four different exposures. Therefore, if the underlying scene radiance is smoothly varying, all four pixels will correspond to roughly the same radiance and the averaging process results in a piece-wise linear response function like the one shown in Figure 4. This response function is obtained by simply adding the response functions for the four exposures shown in Figure 3. The break points between the linear segments are caused by the different saturation points of the individual response functions. Overall, the function in Figure 4 is a gamma-like function with gamma greater than 1. In practice, this simple aggregation method works well except at sharp edges where resolution is slightly reduced.

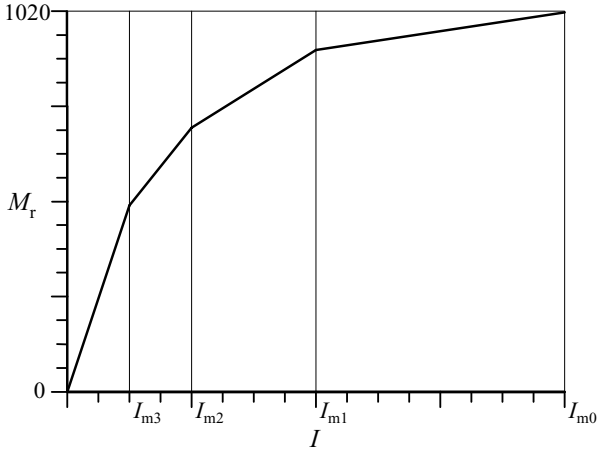

Figure 4: Simple aggregation of the local brightness values produced by the set of different exposures results in an effective response function with a wide dynamic range and a gamma-like non-linearity.

6.2 Image Reconstruction by Interpolation

If our goal is to ensure that the final resolution is close to the actual CCD resolution, a better reconstruction method is needed. For this, we first discard all saturated as well as low intensity (noisy) brightness values using appropriate thresholds. Then, all remaining brightness values $M(i,j)$ are normalized by their respective exposures to obtain the scaled radiance estimates $\tilde{M}(i,j)$.

The reconstruction problem may be posed as one of estimating the discarded brightness values. However, the undiscarded normalized brightness values may themselves be noisy. Therefore, rather than finding estimates for just the discarded brightness values, we find the surface that best fits the undiscarded values and then resample this surface to obtain the complete reconstructed image. For this we define two sets of points in image space, namely, on-grid points that correspond to the pixel locations and off-grid points that lie in between the pixel locations. Our algorithm has two steps. First, we compute all off-grid points from the undiscarded on-grid points. Then, we interpolate all off-grid points to obtain the on-grid ones.

As an example, we use cubic interpolation which is close to the ideal sinc interpolation. Let $M_o(i+0.5, j+0.5)$ be the set of off-grid brightness values located at the centers of all sets of four pixels. If the M_o values were known, the desired on-grid brightnesses $M_r(i,j)$ can be determined by cubic interpolation as: $M_r(i,j) =$

$$\sum_{m=0}^{m=3}\sum_{n=0}^{n=3} f(1.5-m, 1.5-n)\, M_o(i-1.5+m, j-1.5+n) \quad (5)$$

where f is the cubic convolution kernel. We would like to find the M_o values that minimize the error between the normalized measurements and the reconstructed image. If we focus on a specific off-grid point, then (5) can be written in vector form as:

$$\mathbf{M_r} \;=\; \mathbf{F}\,\mathbf{M_o}\,, \quad (6)$$

where, vector $\mathbf{M_r}$ includes 16×1 on-grid brightness val-

ues, matrix $\mathbf{F}$ includes 16×49 cubic convolution kernel elements and vector $\mathbf{M_o}$ includes 49×1 off-grid brightness values. We do not know the on-grid estimates $\mathbf{M_r}$ but rather only the undiscarded on-grid measurements $\tilde{M}(i,j)$. If these measurements are used we get:

$$\tilde{\mathbf{M}} \;=\; \mathbf{F}\,\mathbf{M_o}\,, \tag{7}$$

where, $\tilde{\mathbf{M}}$ is $N \times 16$. Note that $N = 16$ when none of the on-grid measurements are discarded within the span of the interpolation kernel, and $N < 16$ when some of measurements are discarded due to saturation or low intensity. Since this is an underdetermined system of equations, $\mathbf{M_o}$ can be found by using the pseudo-inverse $\mathbf{F}^- = \mathbf{F}^T(\mathbf{F}\mathbf{F}^T)^{-1}$:

$$\mathbf{M_o} \;=\; \mathbf{F}^-\,\tilde{\mathbf{M}}\,. \tag{8}$$

Once all the off-grid brightnesses $M_o(i+0.5, j+0.5)$ have been determined, they can be used in (5) to determine all the on-grid brightness values $M_r(i,j)$ that make up the reconstructed high dynamic range image.

7 Experiments

We are currently developing a prototype SVE camera with on-board image reconstruction capability. Meanwhile, we have conducted several experiments to verify the feasibility of SVE imaging. In these experiments, the SVE image was simulated by combining pixels from four different images taken with exposures $e_k = e_{k-1}R_{k,k-1}$, where $R_{k,k-1}$ are the exposure ratios. It is important to note that the simulated SVE image is exactly what an imaging device would produce with the appropriate optical mask incorporated into it.

Figures 5(a)-(d) show four images captured with a digital camera using the exposure ratios $R_{k,k-1} = 2$. The scene includes two regions that are separated by a panel in the middle that casts a very strong shadow on the right half of the scene, while the left half is brightly lit. As expected, the dark areas produce near-zero (noisy) brightness values in the low exposure image, and saturated brightness values in the high exposure image. In short, none of the four images provide useful brightness values at all pixels. The corresponding SVE image is shown in Figure 5(e) (see inset image for details). The high dynamic range image shown in Figure 5(f) was computed from the SVE image using the aggregation algorithm. This image is brightness enhanced to show that the entire scene is captured despite the significant radiance variations within it.

Figures 5 (g)-(n) show magnified results for a very dark scene region (A) and a very bright region (B). As shown in Figures 5 (g) and (k) the lowest and highest exposures produce poor results for these regions. The best exposures for these regions are different as shown in Figures 5 (h) and (l). For both regions, the output of the SVE method is comparable in brightness quality and resolution to the images produced by the best exposures.

Figures 6 (a)-(d) show four differently exposed images of a scene that includes indoor and outdoor regions. In this case the exposure ratios used were $R_{k,k-1} = 4$. Again, each of these images is either saturated or too dark (noisy) for some part of the scene. The high dynamic range image in Figure 6(f) was computed from the SVE image in Figure 6(e) using the cubic interpolation algorithm. The wide dynamic range of this image was compressed to more effectively display the richness of information captured by the SVE method.

8 Response Function from a Single Image

In our discussions, we have assumed the response function of the imaging system used to construct the SVE system to be linear. However, most imaging systems are non-linear. Measured brightness M is related to the corresponding scaled radiance I as $I = f(M)$, where f is the unknown response function. Methods for computing response functions from multiple images of a scene taken under different exposures have been presented in [Debevec and Malik, 1997] and [Mitsunaga and Nayar, 1999].

We now show that a single SVE image of an arbitrary scene is sufficient to compute the response function f of an imaging system. This results from the fact that embedded within the image are brightness measurements corresponding to different exposures e_k. First, the SVE image, say with four different exposures, is decomposed by subsampling into four images that correspond to different exposures. Then, a simple local brightness variance test is applied to all four images to identify (reliable) pixels that have more or less constant brightness around them. The above decomposition and constancy test result in the mapping of brightness values $M(i,j)$ in the SVE image to values $M_{p,k}$ where $p = 0, 1, ...P$ represent pixel locations in the decomposed image space and $k = 0, 1, ...K$ represent the discrete exposures.

In [Mitsunaga and Nayar, 1999], a polynomial model is used for the response function:

$$I \;=\; f(M) \;=\; \sum_{n=0}^{N} c_n\, M^n \tag{9}$$

where, c_n are the unknown coefficients of the polynomial and N is its order. Since the ratio of scaled radiance for two exposures at the same pixel equals the ratio of the exposures, we have:

$$\frac{I_{p,k}}{I_{p,k-1}} \;=\; R_{k,k-1} \tag{10}$$

where, $R_{k,k-1} = e_k / e_{k-1}$. Substituting (9) in (10) we get an expression where the coefficients c_n of the polynomial are the only unknowns. Using all the stable measurements $M_{p,k}$, the coefficients c_n are estimated by the least-squares method (see [Mitsunaga and Nayar, 1999]).

Figure 7 shows an SVE image that includes four different exposures of the same scene with ratios $R_{k,k-1} = 4$. The above procedure was applied to the image to obtain the response function (solid curve) shown in Figure 8. The accuracy of this function was verified using a calibration color chart with several patches of known reflectances (see circles in Figure 8).

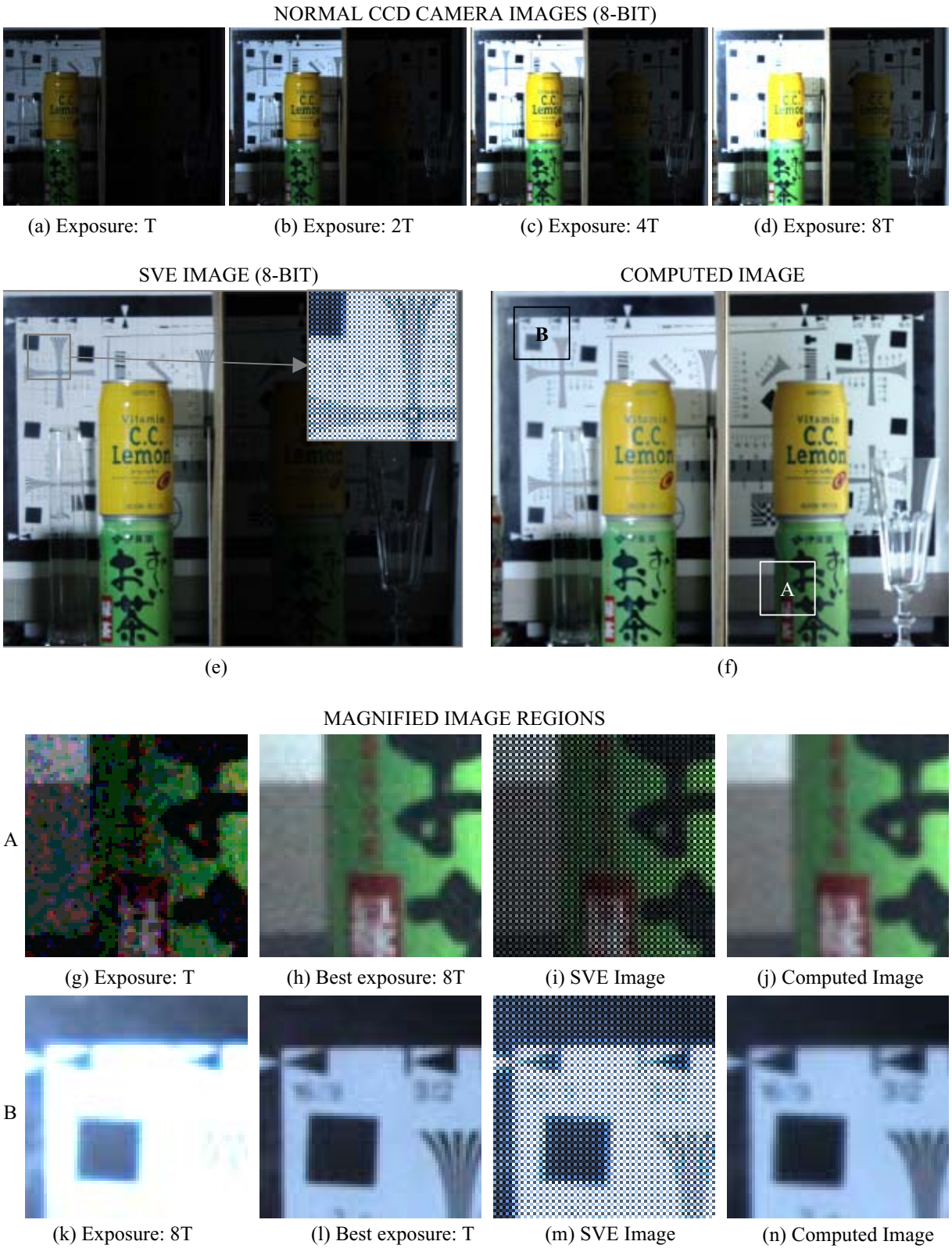

Figure 5: Experimental results on SVE imaging. (a)-(d) Images taken with an 8-bit digital camera using four different exposures. Each image is either too dark (noisy) or saturated for some part of the scene. (e) The corresponding SVE image. (f) The high dynamic range image computed from the SVE image using the aggregation algorithm. This image is histogram equalized to show that the entire range of scene radiances was successfully captured. (g)-(n) Magnified results for regions **A** and **B** shown in image (f). Note that the best exposures (see (h) and (l)) for these regions differ by a factor of 8. Yet, the computed image demonstrates high brightness quality and resolution for both these regions. **(See [CAVE Website, 2000] for color figures)**.

NORMAL CCD CAMERA IMAGES (8-BIT)

(a) Exposure: T

(b) Exposure: 4T

(c) Exposure: 16T

(d) Exposure: 64T

SVE IMAGE (8-BIT)

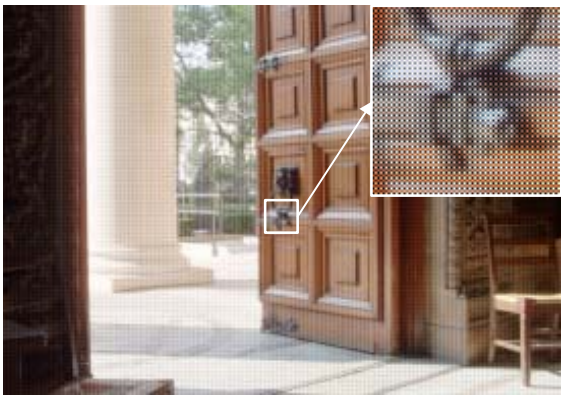

COMPUTED IMAGE

Figure 6: Experimental results on SVE imaging. (a)-(d) Images taken with an 8-bit digital camera using four different exposures. The scene includes indoor (dark) and outdoor (bright) regions. This is a classic example of the type of scene that cannot be captured with any reasonable quality using an 8-bit sensor. All four images are either too dark in the indoor regions or too bright in the outdoor region. (e) The SVE image. (f) The high dynamic range image computed from the SVE image using the cubic interpolation algorithm. Since it hard to print/display the entire dynamic range of the computed image, we have used dynamic range compression to bring out the prominent scene features. **(See [CAVE Website, 2000] for color figures)**.

Figure 7: An SVE image with an exposure pattern that includes four discrete exposures.

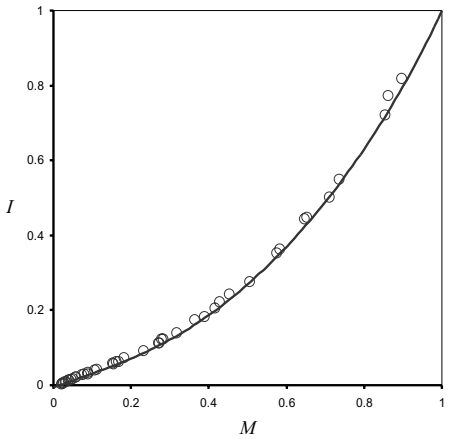

Figure 8: The response function (solid curve) of the imaging system computed from the single SVE image shown in Figure 7. The circles are samples of the response function obtained using a calibration color chart.

References

[Azuma and Morimura, 1996] T. Azuma and A. Morimura. Image composite method and image composite device. Japanese Patent 08-154201, June 1996.

[Blackwell, 1946] H. R. Blackwell. Contrast thresholds of the human eye. *Journal of the Optical Society of America*, 36:624–643, 1946.

[Brajovic and Kanade, 1996] V. Brajovic and T. Kanade. A Sorting Image Sensor: An Example of Massively Parallel Intensity-to-Time Processing for Low-Latency Computational Sensors. *Proc. of IEEE Conference on Robotics and Automation*, pages 1638–1643, April 1996.

[Burt and Kolczynski, 1993] P. Burt and R. J. Kolczynski. Enhanced Image Capture Through Fusion. *Proc. of International Conference on Computer Vision (ICCV)*, pages 173–182, 1993.

[CAVE Website, 2000] S. K. Nayar and T. Mitsunaga. High dynamic range imaging: Spatially varying pixel exposures. *http://www.cs.columbia.edu/CAVE/*, March 2000.

[Debevec and Malik, 1997] P. Debevec and J. Malik. Recovering High Dynamic Range Radiance Maps from Photographs. *Proc. of ACM SIGGRAPH 1997*, pages 369–378, 1997.

[Doi *et al.*, 1986] H. Doi, Y. Hara, Y. Kenbo, and M. Shiba. Image sensor. Japanese Patent 08-223491, August 1986.

[Hamazaki, 1996] M. Hamazaki. Driving method for solid-state image pickup device. Japanese Patent 08-331461, December 1996.

[Handy, 1986] R. J. Handy. High dynamic range ccd detector/imager. U.S. Patent 4623928, November 1986.

[Healey and Kondepudy, 1994] G. Healey and R. Kondepudy. Radiometric CCD Camera Calibration and Noise Estimation. *IEEE Trans. on Pattern Analysis and Machine Intelligence*, 16(3):267–276, March 1994.

[Ikeda, 1998] E. Ikeda. Image data processing apparatus for processing combined image signals in order to extend dynamic range. U.S. Patent 5801773, September 1998.

[Kimura, 1998] T. Kimura. Image pickup device. Japanese Patent 10-069011, March 1998.

[Konishi *et al.*, 1995] M. Konishi, M. Tsugita, M. Inuiya, and K. Masukane. Video camera, imaging method using video camera, m ethod of operating video camera, image processing apparatus and method, and solid-state electronic imaging device. U.S. Patent 5420635, May 1995.

[Madden, 1993] B. Madden. Extended Intensity Range Imaging. Technical Report MS-CIS-93-96, Grasp Laboratory, University of Pennsylvania, 1993.

[Mann and Picard, 1995] S. Mann and R. Picard. Being 'Undigital' with Digital Cameras: Extending Dynamic Range by Combining Differently Exposed Pictures. *Proc. of IST's 48th Annual Conference*, pages 442–448, May 1995.

[Mitsunaga and Nayar, 1999] T. Mitsunaga and S. K. Nayar. Radiometric Self Calibration. In *Proc. of Computer Vision and Pattern Recognition '99*, volume 1, pages 374–380, June 1999.

[Morimura, 1993] A. Morimura. Imaging method for a wide dynamic range and an imaging device for a wide dynamic range. U.S. Patent 5455621, October 1993.

[Murakoshi, 1994] M. Murakoshi. Charge coupling image pickup device. Japanese Patent 59-217358, December 1994.

[Saito, 1995] K. Saito. Electronic image pickup device. Japanese Patent 07-254965, February 1995.

[Saito, 1996] K. Saito. Electronic image pickup device. Japanese Patent 08-340486, December 1996.

[Street, 1998] R. A. Street. High dynamic range segmented pixel sensor array. U.S. Patent 5789737, August 1998.

[Takahashi *et al.*, 1997] K. Takahashi, T. Hieda, C. Satoh, T. Masui, T. Kobayashi, and K. Yoshimura. Image device with diverse storage times used in picture composition. U.S. Patent 5638118, June 1997.

[Theuwissen, 1995] A. J. P. Theuwissen. *Solid State Imaging with Charge-Coupled Devices*. Kluwer Academic Press, Boston, 1995.

[Tsai, 1994] Y. T. Tsai. Method and apparatus for extending the dynamic range of an electronic imaging system. U.S. Patent 5309243, May 1994.

[Wen, 1989] D. D. Wen. High dynamic range charge coupled device. U.S. Patent 4873561, October 1989.